Electronic Supporting Information

The role of Ag in the aqueous solution processed $(Ag,Cu)_2ZnSn(S,Se)_4$ kesterite solar cells: antisite defects elimination and importance of Na passivation

Wei-Chih Huang,‡[a] Shih-Yuan Wei,‡[a] Chung-Hao Cai[a], Wei-Hao Ho[a] and Chih-Huang Lai[a,]*

[a.] Department of Materials Science and Engineering, National Tsing Hua University, No. 101, Section 2, Kuang-Fu Road, Hsinchu, Taiwan 30013, R.O.C.

* E-mail: chlai@mx.nthu.edu.tw

‡Authors contributed equally to this work.

Table S1. Summary of chemical concentrations for the source of Ag, Cu, Zn, Sn and S in precursor solutions.

Sample No.	$CuCl_2 \cdot 2H_2O$	$AgNO_3$	$SnCl_2$	$Zn(NO_3)_2 \cdot 6H_2O$	Thiourea
CZTSSe	22.6 mM	0	12.0 mM	14.7 mM	213 mM
Ag 10	20.3 mM	2.3 mM	12.0 mM	14.7 mM	213 mM
Ag 20	18.1 mM	4.5 mM	12.0 mM	14.7 mM	213 mM
Ag 35	14.7 mM	7.9 mM	12.0 mM	14.7 mM	213 mM
Ag 50	11.3 mM	11.3 mM	12.0 mM	14.7 mM	213 mM
AZTSSe	0	22.6 mM	12.0 mM	14.7 mM	213 mM

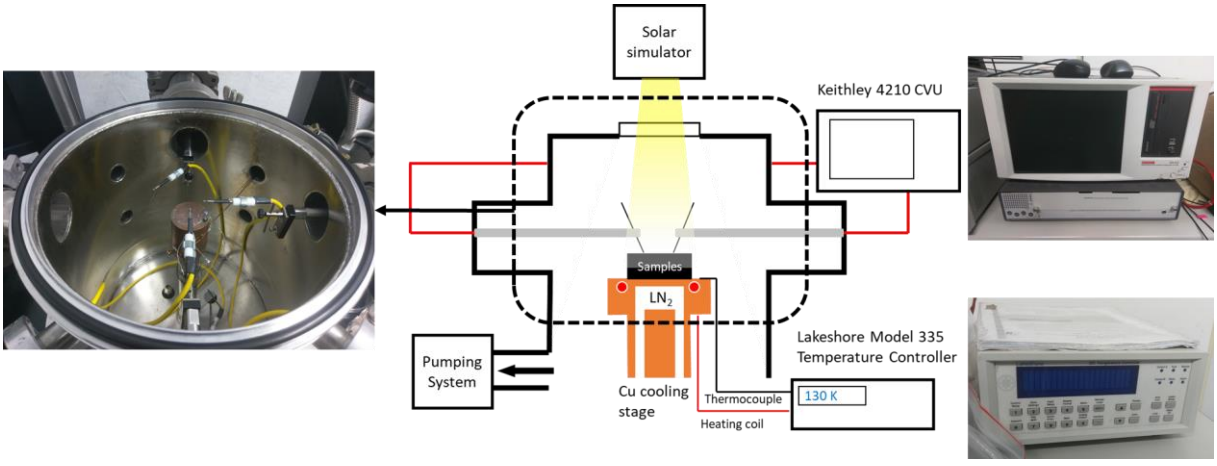

Fig. S1 The schematic diagram of the low temperature measurements.

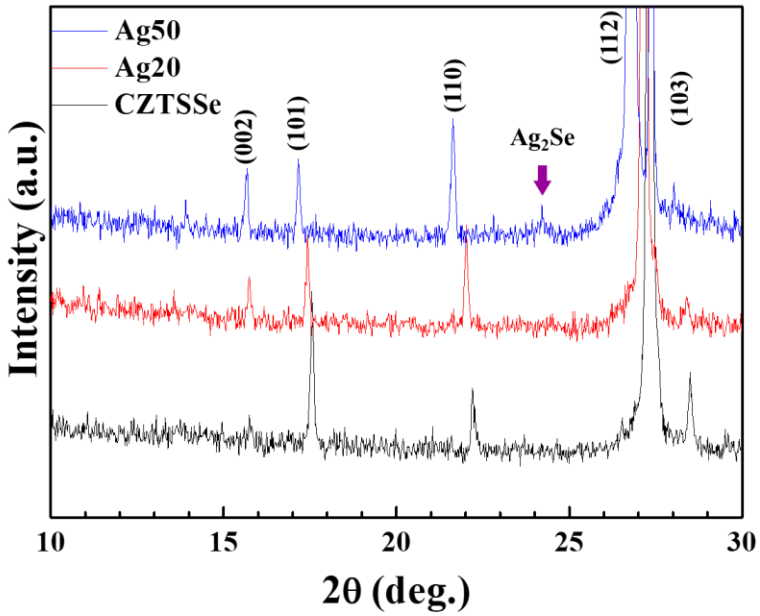

Fig. S2 The XRD of CZTSSe, Ag 20 and Ag 50 annealed under 550 °C. The Ag_2Se is observed as the secondary phase in Ag 50.

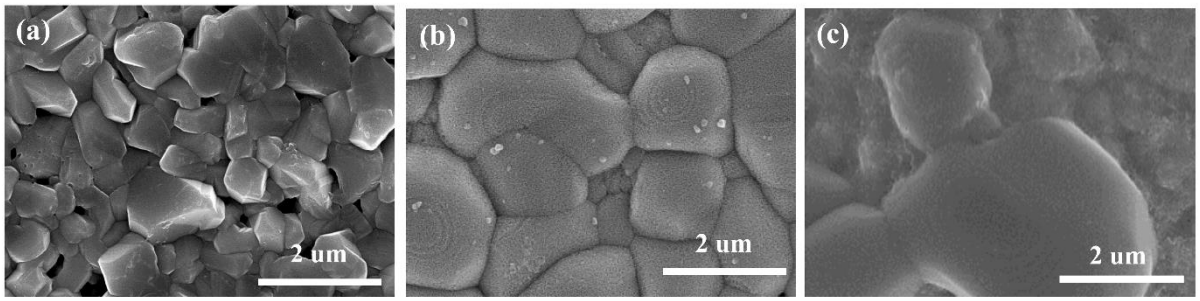

Fig. S3 The plane-view SEM images of (a) CZTSSe, (b) Ag 20 and (c) Ag 50 annealed at 550 °C. Larger grains are obtained in Ag 20 compared with CZTSSe. The aggregated grains are observed in Ag 50 at high annealing temperature.

Table S2 The results of EDX composition analysis for ACZTSSe films after annealing process

Sample No.	M_I/(Zn+Sn)	Zn/Sn	S/(S+Se)	Ag/M_I
CZTSSe	0.824	1.252	0.072	0
Ag 20	0.862	1.167	0.083	0.198
Ag 35	0.861	1.194	0.082	0.345
Ag 50	0.883	1.239	0.047	0.455
AZTSSe	0.865	1.194	0.047	1

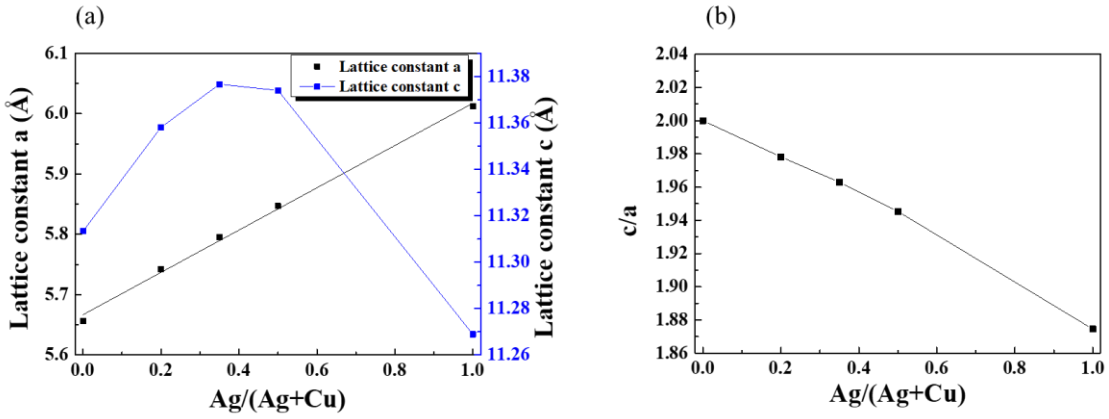

Fig. S4 (a) Refined lattice constant along a-axis and c-axis. (b) c/a ratio of ACZTSSe with different Ag/(Ag+Cu) ratio.

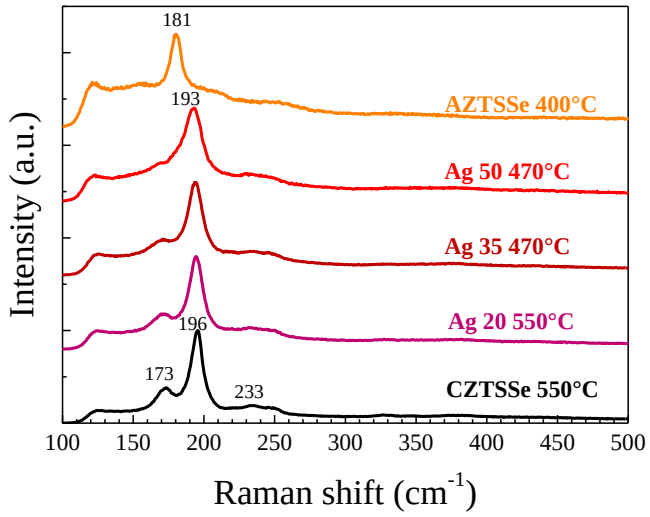

Fig. S5 The Raman spectra of ACZTSSe with different Ag content.

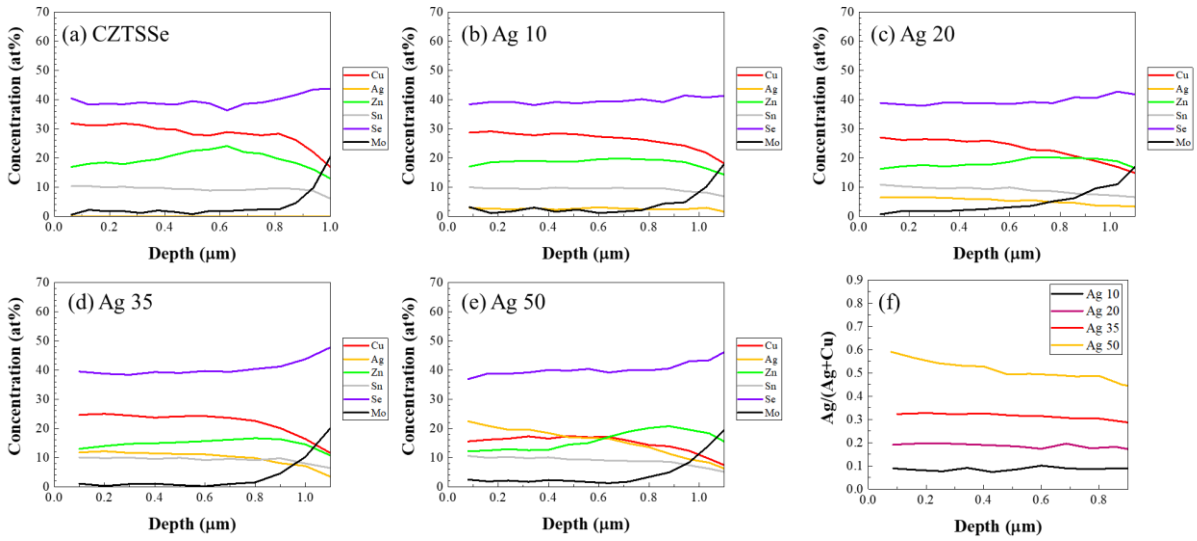

Fig. S6 XPS depth profiles of the (a) CZTSSe (b) Ag 10 (c) Ag 20 (d) Ag 35 (e) Ag 50 and (f) the distribution of Ag/(Ag+Cu) ratio.

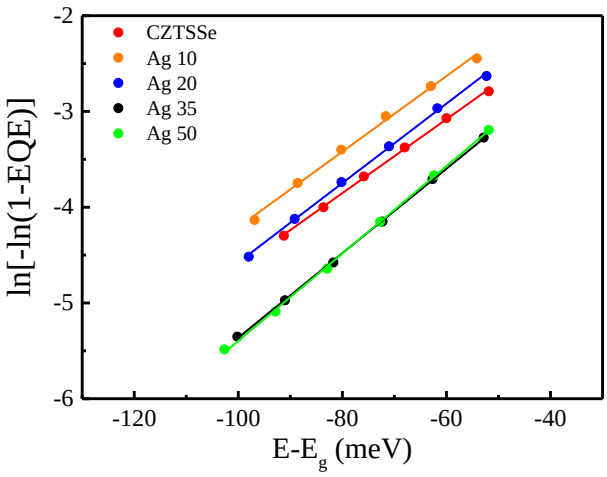

Fig. S7 Linear fitting of the ln[-ln[1-EQE]] for the Urbach tail analysis.

Table S3 The linear fitting results of the slope to deduce the Urbach tail energy

Sample No.	Slope	R^2	E_U (meV)
CZTSSe	38.58 ±0.51	0.999	25.9
Ag 10	39.47 ±1.19	0.995	25.3
Ag 20	41.48 ±0.68	0.998	24.1
Ag 35	44.12 ±0.41	0.999	22.7
Ag 50	45.61 ±0.56	0.999	21.9

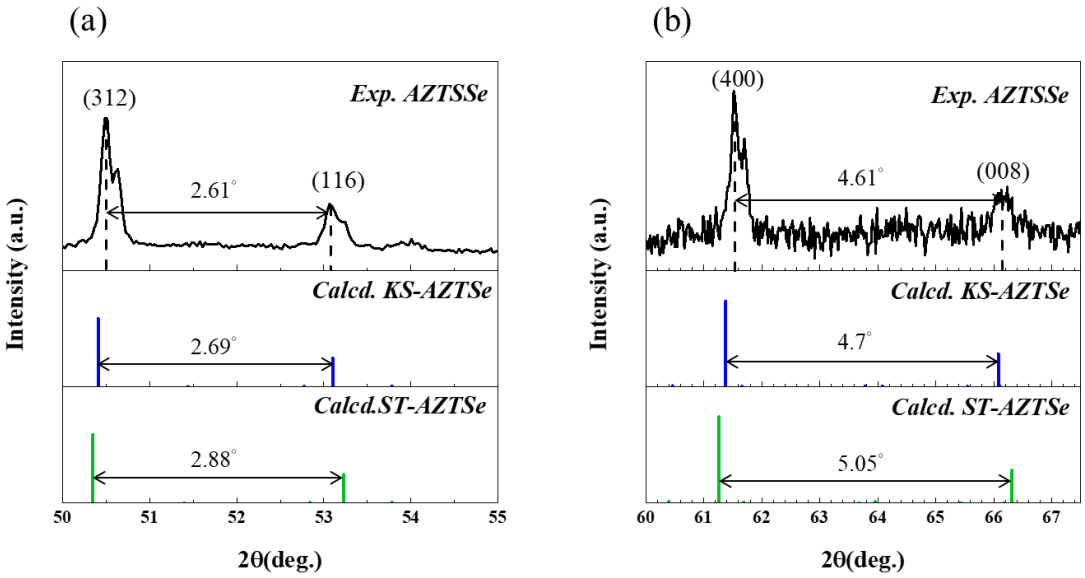

Fig. S8 The diffraction pattern of the experimental AZTSSe, calculated kesterite (KS) and stannite (ST) AZTSe ranging from (a) 50° to 55° corresponding to (312) and (116) and (b) 60° to 67.5° corresponding to (400) and (008) characteristic peaks. The satellite peaks correspond to the $K\alpha_2$ radiation.

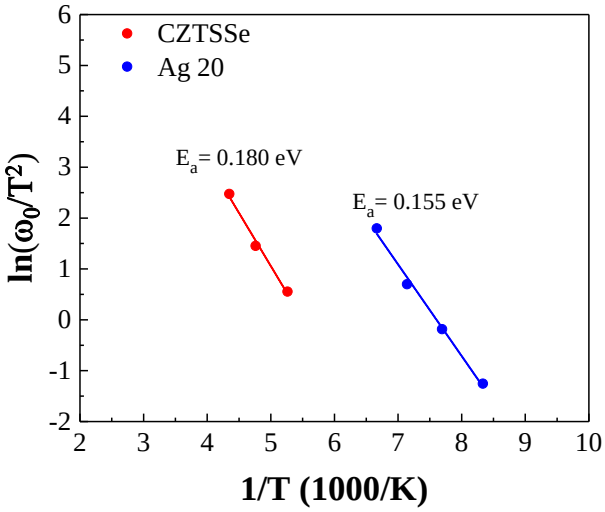

Fig. S9 The Arrhenius plot of step frequency determined from the admittance spectra of CZTSSe and Ag 20.

Quantitative calculations of the defect density (N_T)

$$\omega = 2\pi f = N_V \upsilon_{th} \sigma_{n.p} e^{-E_\omega/kT} = 2\xi_0 T^2 e^{-E_\omega/kT} \quad \text{(S1)}$$

$$E_\omega = E - E_V = kTln(\frac{2\xi_0 T^2}{\omega}) \quad \text{(S2)}$$

$$N_T(E_\omega) = -\frac{2V_{bi}^{\frac{3}{2}}}{WkT\sqrt{q}\sqrt{qV_{bi}-(E_g-E_\omega)}}\frac{dC}{dln\omega} \quad \text{(S3)}$$

Where ω is the angular frequency, E_ω is an energy related to the temperature and drive frequency and could be converted as the energy difference from valence band maximum (E_V), the $\boldsymbol{\xi_0}$ is the pre-exponential factor including the temperature-independent terms of defect capture cross section $\boldsymbol{\sigma_{n.p}}$, effective density of states in the valence band $\boldsymbol{N_V}$, and the thermal velocity $\boldsymbol{\upsilon_{th}}$. The V_{bi}, C, W, k, q and E_g are the built-in-potential, capacitance, depletion width, Boltzmann constant, element charge and band gap, respectively. Fig. 5(d) and Fig. 5(e) can be plotted by following the Equation S2 and Equation S3.

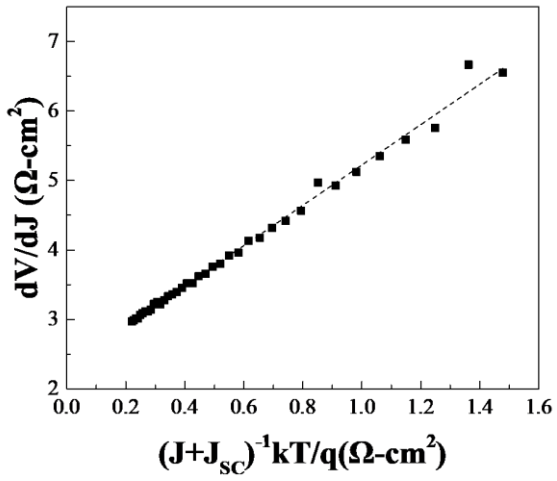

Fig. S10 An example of ideality factor fitting of CZTSSe at 300 K.

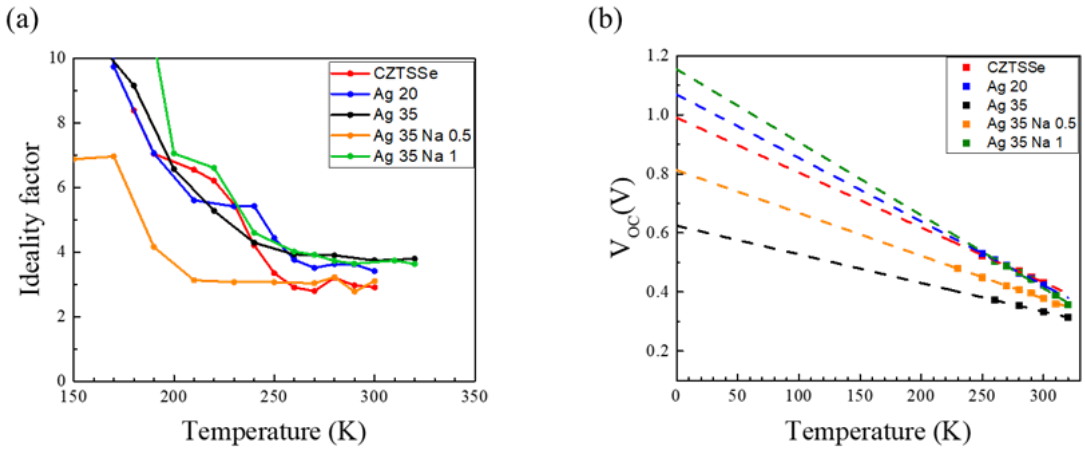

Fig. S11 (a) The ideality factor vs. temperature for various samples. (b) Linear fitting of V_{OC} vs temperature to get activation energy.

Table S4 The linear fitting results of the V_{OC}-T to deduce the activation energy.

Sample	R^2	E_a (eV)
CZTSSe	0.996	0.990±0.015
Ag 20	0.999	1.069±0.006
Ag 35	0.999	0.624±0.002
Ag 35 Na 0.5at%	0.996	0.812±0.010
Ag 35 Na 1at%	0.989	1.154±0.033

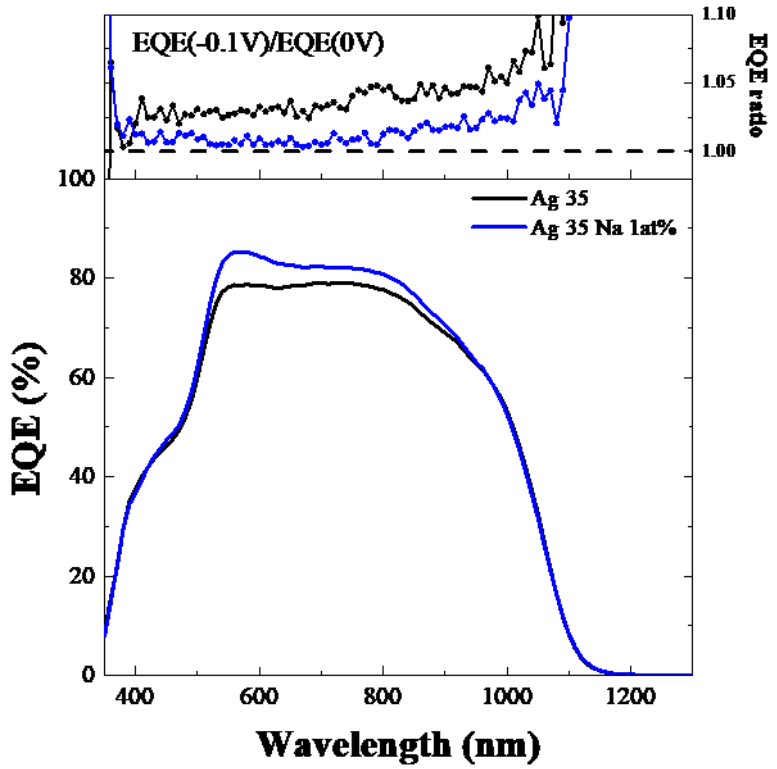

Fig. S12 The EQE spectra of Ag 35 with or without Na and the EQE ratio as -0.1 V was applied.

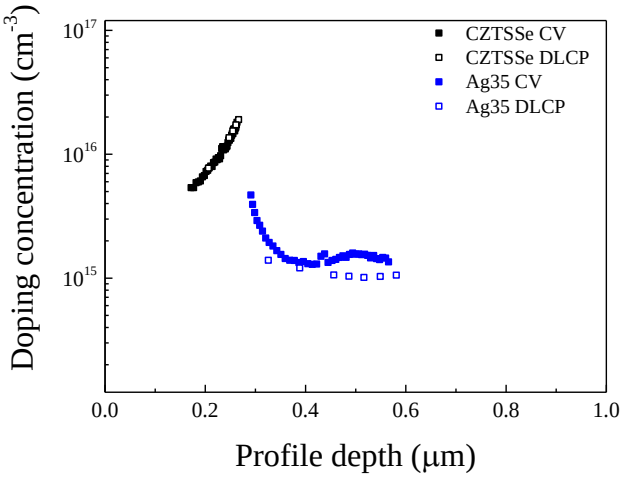

Fig. S13 The doping concentration of CZTSSe and Ag 35 without additional Na derived from C-V (solid dots) and DLCP (empty dots).

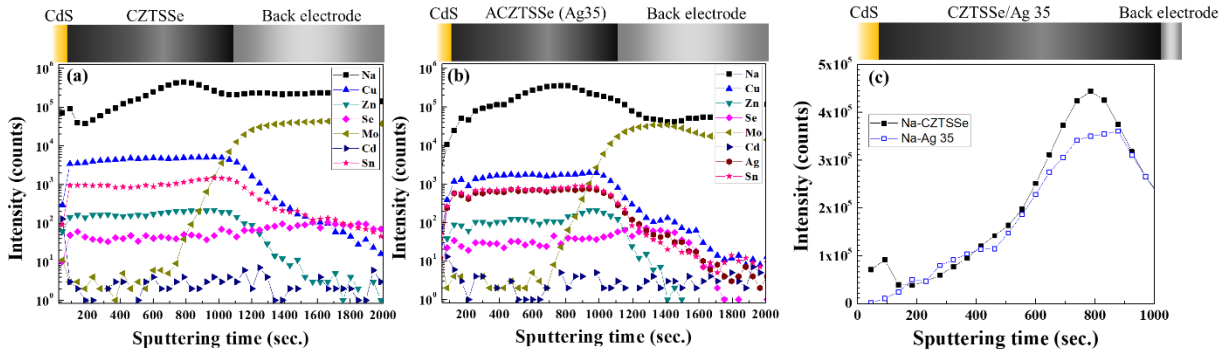

Fig. S14 SIMS depth profiles of the (a) CZTSSe (b) ACZTSSe (Ag 35, without extra Na) solar cells and (c) the comparison of Na profile for both samples in linear scale. Before SIMS analysis, the devices were etched in HCl solution to remove the window layer.

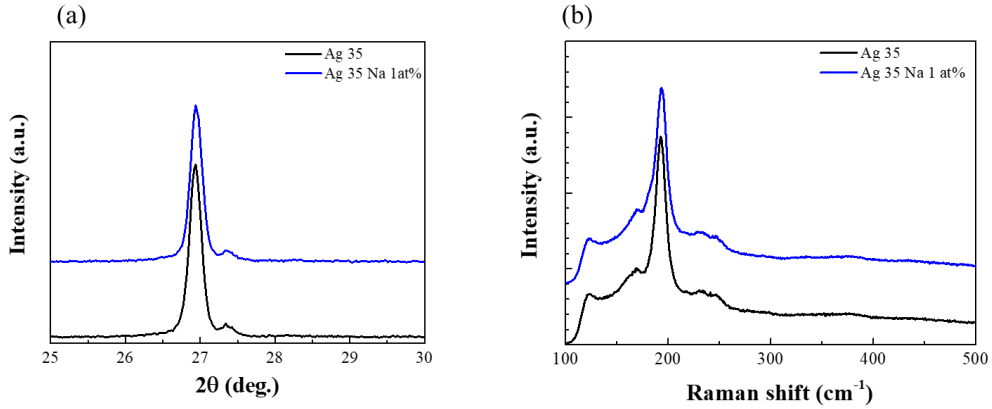

Fig. S15 (a) (112) X-ray diffraction pattern and (b) Raman spectra of Ag 35 with or without 1 at% Na addition.

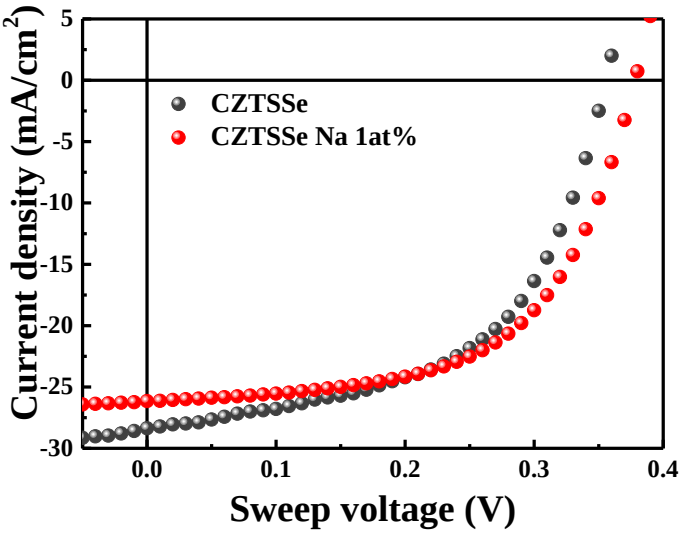

Fig. S16 The comparison of J-V characteristics for the CZTSSe solar cell with or without extra Na addition.

Table S5 Summarized device parameters of CZTSSe with different amount of Na incorporation.

Sample No.	V_{OC} (mV)	J_{SC} (mA/cm^2)	Fill factor (%)	Efficiency (%)	Carrier density (#/cm^3)
w/o extra Na	357 ± 11	-28.41 ± 0.35	53.6 ± 5.8	5.65 ± 0.69	1.46×10^{16}
Na 1%	380 ± 4	-26.04 ± 0.50	58.0 ± 1.0	5.72 ± 0.13	3.27×10^{16}